Expansion of oil palm and other cash crops causes an increase of the land surface temperature in the Jambi province in Indonesia

Clifton R. Sabajo[1,2†], Guerric le Maire[3], Tania June[4], Ana Meijide[1], Olivier Roupsard[3,5], Alexander Knohl[1,6]

[1] University of Goettingen, Bioclimatology, 37077 Göttingen, Germany

[2] AgroParisTech – Centre de Montpellier, Agropolis International, 648 rue Jean-François Breton, 34093 Montpellier, France

[3] CIRAD, UMR Eco&Sols, F-34398 Montpellier, France

[4] Agrometeorology Laboratory Department of Geophysics and Meteorology, Faculty of Mathematics and Natural Sciences, Bogor Agricultural University (IPB), Indonesia

[5] CATIE (Centro Agronómico Tropical de Investigación y Enseñanza / Tropical Agriculture Centre for Research and Higher Education), 7170 Turrialba, Costa Rica

[6] University of Goettingen, Centre of Biodiversity and Sustainable Land Use (CBL), 37073 Goettingen, Germany

[†] Correspondence: Clifton R. Sabajo, University of Goettingen, Bioclimatology, Büsgenweg 2, 37077 Göttingen, Germany. E-mail: csabajo@uni-goettingen.de

Telephone: +49 (0) 551 39 12114

Abstract

Indonesia is currently one of the regions with the highest transformation rate of the land surface worldwide related to the expansion of oil palm plantations and other cash crops replacing forests on large scales. Land cover changes, which modify land surface properties, have a direct effect

on the land surface temperature (LST), a key driver for many ecological functions. Despite the large historic land transformation in Indonesia toward oil palm and other cash crops and governmental plans for future expansion, this is the first study so far to quantify the impacts of land transformation on the LST in Indonesia. We analyse LST from the thermal band of a Landsat image and produce a high-resolution surface temperature map (30m) for the lowlands of the Jambi province in Sumatra (Indonesia), a region which suffered large land transformation towards oil palm and other cash crops over the past decades. The comparison of LST, albedo, Normalized Differenced Vegetation Index (NDVI), and evapotranspiration (ET) between seven different land cover types (forest, urban areas, clear cut land, young and mature oil palm plantations, acacia and rubber plantations) shows that forests have lower surface temperatures than the other land cover types, indicating a local warming effect after forest conversion. LST differences were up to 10.1 ± 2.6 ºC (mean ± SD) between forest and clear-cut land. The differences in surface temperatures are explained by an evaporative cooling effect, which offsets the albedo warming effect. Our analysis of the LST trend of the past 16 years based on MODIS data, shows that the average daytime surface temperature in the Jambi province increased by 1.05 ºC, which followed the trend of observed land cover changes and exceed the effects of climate warming. This study provides evidence that the expansion of oil palm plantations and other cash crops leads to changes in biophysical variables, warming the land surface and thus enhancing the increase of the air temperature because of climate change.

Keywords: Land surface temperature, albedo, NDVI, evapotranspiration, biophysical variables, oil palm, remote sensing, Landsat, MODIS, Indonesia, land-use / land cover change

1 Introduction

Indonesia is one of the regions where the expansion of cash crop monocultures such as acacia (timber plantations), rubber, oil palm plantations and smallholder agriculture has drastically reduced the area of primary forest in the last two and a half decades (Bridhikitti and Overcamp, 2012; Drescher et al., 2016; Marlier et al., 2015; Miettinen et al., 2012; Verstraeten et al., 2005). This large scale conversion of rainforest for agricultural use has been observed on the island of Sumatra, which has experienced the highest primary rainforest cover loss in all of Indonesia (Drescher et al., 2016; Margono et al., 2012; Miettinen et al., 2011). Forest cover in the Sumatran provinces of Riau, North Sumatra and Jambi, declined from 93 to 38% of provincial area between 1977 and 2009 (Miettinen et al., 2012). These large scale transformations, observed as land cover change, and land-use intensification have led to substantial losses in animal and plant diversity, ecosystem functions and changed microclimatic conditions (Clough et al., 2016; Dislich et al., 2016; Drescher et al., 2016). Additionally, these changes directly alter vegetation cover and structure and land surface properties such as albedo, emissivity, and surface roughness which affect gas and energy exchange processes between the land surface and the atmosphere (Bright et al., 2015).

Replacing natural vegetation with another land cover modifies the surface albedo, which affects the amount of solar radiation that is absorbed or reflected and consequently alters net radiation and local surface energy balance. A lower or higher albedo results in a smaller or greater reflection of shortwave radiation. As a result, the higher or lower amounts of net radiation absorption may increase or decrease the surface temperature and change evapotranspiration (Mahmood et al., 2014).

Changes in land cover also alter surface emissivity, i.e. the ratio of radiation emitted from a surface to the radiation emitted from an ideal black body at the same temperature following the Stefan–Boltzmann law. Emissivity of vegetated surfaces varies with plant species, density, growth stage, water content and surface roughness (Snyder et al., 1998; Weng et al., 2004). A change of emissivity affects the net radiation because it determines the emission of longwave radiation that contributes to radiative cooling (Mahmood et al., 2014).

Water availability, surface type, soil humidity, local atmospheric and surface conditions affect the energy partitioning into latent (LE), sensible (H) and ground heat (G) fluxes (Mildrexler et al., 2011). Surface roughness affects the transferred sensible and latent heat by regulating vertical mixing of air in the surface layer (van Leeuwen et al., 2011) thereby regulating land surface temperature (LST). Through its association with microclimate, net radiation and energy exchange (Coll et al., 2009; Sobrino et al., 2006; Voogt and Oke, 1998; Weng, 2009; Zhou and Wang, 2011), LST is a major land surface parameter and as climatic factor it is regarded a main driver of diversity gradients related to the positive relationships between temperature and species richness (Wang et al., 2016).

The replacement of natural vegetation also changes evapotranspiration (ET) (Boisier et al., 2014) and LST because the surface biophysical variables (i.e. surface albedo, LST, emissivity and indirectly Leaf Area Index (LAI) and Normalized Difference Vegetation Index (NDVI)) are interconnected through the surface radiation balance. When ET decreases for example, surface temperatures and sensible heat (H) fluxes increase; on the other hand, when ET increases, the increased LE fluxes lower surface temperatures and decrease H fluxes (Mahmood et al., 2014) under equal net radiation conditions because with a change in vegetation, soil and ecosystem heat flux and net radiation also change due to an alteration of the biophysical variables. Vegetation structure, represented by NDVI, LAI and vegetation height, is in this

104 respect an important determinant of the resistances or conductivities to heat, moisture, and
105 momentum transfer between the canopy and the atmosphere (Bright et al., 2015) facilitating the
106 amounts/ratios of sensible heat to water vapour dissipation away from the surface (Hoffmann
107 and Jackson, 2000).
108
109 To understand the effects of land cover changes on LST, the associated biophysical variables
110 must be evaluated. This can be done through the surface radiation budget and energy
111 partitioning which unites these biophysical variables directly or indirectly: albedo as direct
112 determinant of the net solar radiation, NDVI as a vegetation parameter determining the
113 emissivity, which in turn determines the amount of reflected and emitted longwave radiation,
114 LST directly affecting the amount of emitted longwave radiation from the surface and ET,
115 which affects the amount of energy that is used for surface cooling via evaporating of water.
116
117 The effect of land cover change on LST is dependent on the scale, location, direction and type
118 of the change (Longobardi et al., 2016). Several studies showed an LST increase after forest
119 conversion to built-up areas, agricultural land (Zhou and Wang, 2011), crop land and pasture
120 lands (Peng et al., 2014) in China. Similar observations were reported for South American
121 ecosystems: low vegetation such as grasslands in Argentina were warmer than tall tree
122 vegetation (Nosetto et al., 2005). In Brazil, the surface temperature increased after the
123 conversion of natural Cerrado vegetation (a savanna ecosystem) into crop/pasture (Loarie et al.,
124 2011a). Similar effects were also observed for other South American biomes (Salazar et al.,
125 2016). In a global analysis, Li et al. (2015) showed that the cooling of forests is moderate at
126 mid latitudes but Northern boreal forests are warmer, an indication that the effect of land cover
127 change on LST varies with the location of the land cover change (Longobardi et al., 2016).
128 Similar studies on the Indonesian Islands are lacking but surface temperature increases are
129 expected as an effect of oil palm and cash crop land expansion in the recent decades.

Measuring LST changes is critical for understanding the effects of land cover changes, but challenging. LST can be monitored with LST products retrieved from thermal infrared (TIR) remote sensing data e.g. the use of the thermal bands of the Moderate Resolution Imaging Spectrometer (MODIS) onboard the Terra and Aqua satellite (Sobrino et al., 2008), the thermal band of the Thematic Mapper (TM) onboard the LANDSAT-5 platform (Sobrino et al., 2004, 2008) or Enhanced Thematic Mapper (ETM+) onboard the LANDSAT-7 platform. The advantage of MODIS data is the availability of readily processed products at high temporal resolution (daily) at medium (250 – 500 m) to coarse (1000 – 5000 m) spatial resolution scale; MODIS LST product (MOD11A1/MYD11A1) for example is provided at a daily temporal resolution with a spatial resolution of 1 km. Landsat data are provided at a higher spatial resolution (30 m), but the temporal resolution is however limited to 16 days and the retrieval of LST requires the correction of the satellite observed radiances for atmospheric absorption and emission (Coll et al., 2009). Besides LST, the connected biophysical variables of the energy and radiation budget can be derived from the visible and near-infrared (VIS-NIR) bands of MODIS or Landsat, making integrated monitoring of the biophysical variables related to changing land surface possible. In Indonesia, a large proportion of the land use changes is driven by smallholders (Dislich et al., 2016), thus a combination of Landsat (for a fine spatial resolution) and MODIS (for temporal developments) seems desirable.

The modification of the physical land surface properties influences climate and local microclimatic conditions via biogeochemical and biophysical processes. Therefore, given Indonesia's history of large scale agricultural land conversion and governmental plans to substantially expand the oil palm production (Wicke et al., 2011), it is important to study the effects of the expansion of cash crop areas on the biophysical environment, especially on LST as a key land surface parameter. These effects have been poorly studied in this region and

according to our knowledge this is the first study to quantify the effects of land use change on LST in Indonesia. We focus on the Jambi province (on Sumatra/Indonesia) as it experienced large land transformation towards oil palm and other cash crops such as rubber plantations in the past and it may serve as an example of future changes in other regions.

Our main objective is to quantify the differences in LST across different land cover types and to assess the impact of cash crop expansion on the surface temperature in the Jambi province in the past decades (2000 – 2015). With this study we aim to (1) evaluate the use of Landsat and MODIS satellite data as sources for a reliable surface temperature estimation in a tropical region with limited satellite data coverage by comparing the surface temperatures retrieved from both satellite sources to each other and against ground observations, (2) to quantify the LST variability across different land cover types and (3) to assess the long term effects of land transformation on the surface temperature against the background of climatic changes and (4) to identify the mechanisms that explain the surface temperature changes caused by alterations of biophysical variables. In this study we compare the surface temperatures of different land cover types that replace forests (i.e. oil palm, rubber and acacia plantations, clear cut land and urban areas) by using high resolution Landsat and medium resolution MODIS satellite data and discuss the differences by taking into account other biophysical variables such as the albedo, NDVI and evapotranspiration (ET).

2 Materials and methods

2.1 Study area

The study was carried out in the lowlands (approx. 25 000 km^2) of the Jambi province (total area 50 160 km^2) on Sumatra, Indonesia, between latitudes 0°30´S and 2°30´S and longitudes

101°E and 104°30´E (Fig. 1). This region has undergone large land transformation towards oil palm and rubber plantations over the past decades and thus may serve as an example of expected changes in other regions of Indonesia (Drescher et al., 2016). The area has a humid tropical climate with a mean annual temperature of 26.7 ± 0.2 °C (1991 – 2011, annual mean ± SD of the annual mean), with little intra-annual variation. Mean annual precipitation was 2235 ± 381 mm and a dry season with less than 120 mm monthly precipitation usually occurred between June and September (Drescher et al., 2016). Previously logged rainforests in the Jambi province have been converted to intensively managed agro-industrial production zones and into smallholder farms to grow cash crops of rubber (*Hevea brasiliensis*) and oil palm (*Elaeis guineensis*) or fast-growing tree species such as *Acacia mangium* for pulp production (Drescher et al., 2016). The area cultivated with oil palm grew faster than the area cultivated with rubber plantations between 1990 and 2011 (Clough et al., 2016).

For this study, we used two data sets of different plot sizes. For the first data set, we delineated 28 large plots (ranging from 4 to 84 km^2) of 7 different land cover types (Forest (FO), Rubber (RU), Acacia Plantation Forest (PF), Young oil palm plantation (YOP), Mature Oil Palm Plantation (MOP), Urban area (UB) and Clear-Cut areas (CLC)) (Fig. 1). The delineation was based on visual interpretation in combination with field observations, which were conducted between October – December 2013. The large size of the plots was necessary to make a comparison between MODIS and Landsat images (see section satellite data). For the second data set, we selected 49 smaller plots within and outside these 28 large plots (between 50 × 50 m and 1000 × 1000 m) (Fig. 1) which allowed us to increase the number of plots to use when analysing Landsat images. These small plots were used to extract the surface temperature (LST), Normalized Difference Vegetation Index (NDVI), albedo (α) and evapotranspiration (ET) from a high resolution Landsat satellite image (see section satellite data) for the 7 different land cover types of interest.

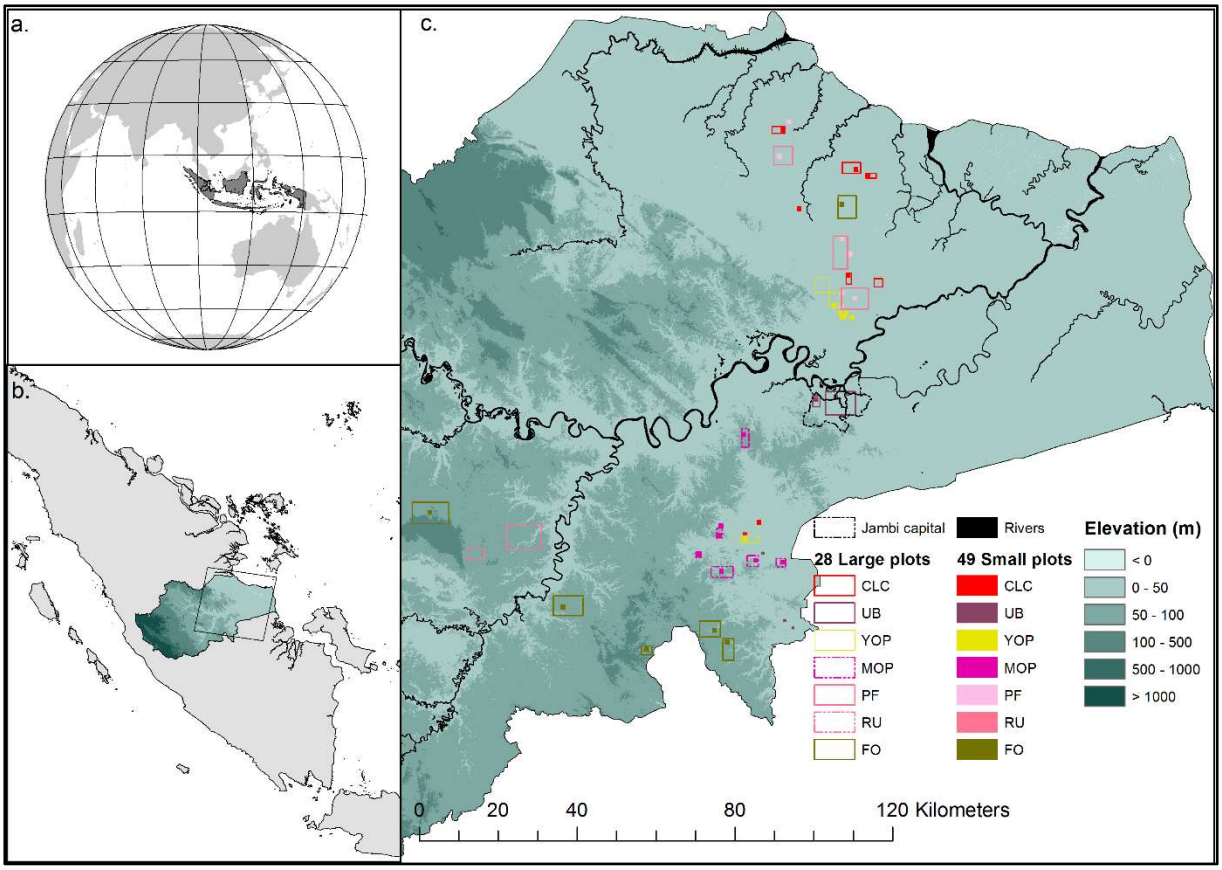

Fig. 1 Geographic location of the study area. Jambi province on the Sumatran Island of Indonesia (Figs. 1a and 1b). The background of the map (Fig. 1c) is a digital elevation model, showing that the plots are located in the lowlands of the Jambi province. The large rectangles are the 28 different land cover types (Forest, Young and Mature Oil palm, Rubber, Urban area, Acacia Plantation Forest and Clear-Cut land), the small squares are the locations of the 49 small plots of the 7 different land cover types. Abbreviations: CLC = Clear-cut land, UB = Urban area, YOP = Young oil palm plantation, MOP = Mature Oil Palm plantation, PF = Acacia plantation forest, RU = Rubber plantation, FO = Forest.

2.2 Meteorological data

Air temperature and relative air humidity were measured at four reference meteorological stations located in open areas within the study area (Drescher et al., 2016), with thermohygrometers (type 1.1025.55.000, Thies Clima, Göttingen, Germany) placed at 2m height. Measurements were recorded every 15 s and then averaged and stored in a DL16 Pro

data logger (Thies Clima, Göttingen, Germany) as 10 min mean, from February 2013 to December 2015. We used the air temperature from the meteorological stations to compare to MODIS air temperatures (MOD07_L2). The relative air humidity was used as an input parameter for NASA's online atmospheric correction (ATCOR) parameter tool to derive parameters to correct Landsat thermal band for atmospheric effects (see Satellite data). We also used air temperature and relative humidity from two eddy covariance flux towers located in the study area (Meijide et al., 2017): one in a young oil palm plantation (two years old, S 01°50.127', E 103°17.737'), and the other one in a mature oil palm plantation (twelve years old, S 01°41.584', E 103°23.484'). At these flux towers, air temperature and relative humidity were measured above the canopy respectively with the same instruments as in the reference meteorological stations (see Meijide et al. (2017), for a description of the methodology). At the flux tower located in the mature oil palm plantation, we also measured the surface canopy temperature between August 2014 and December 2015, which was compared to MODIS LST estimates from the same period. The canopy temperature was measured with two infrared sensors (IR100) connected to a data logger, (CR3000) both from Campbell Scientific Inc. (Logan, USA). For a regional coverage we used ERA Interim daily air temperature grids (http://apps.ecmwf.int/datasets/data/interim-full-daily/levtype=sfc/; (Dee et al., 2011) from 2000 – 2015 at 0.125 degrees resolution to study the annual air temperature trend in this period.

2.3 Satellite data

A Landsat 7 ETM+ VIS/TIR 30 m resolution surface reflectance image with low cloud cover, acquired at 10:13 hours (local time) on 19 June 2013 covering the lowland area of the Jambi province (path 125, row 61) was used in this study. Like all Landsat 7 ETM+ images acquired after 31 May 2003, the image we used was affected by a scan line error causing a data loss of about 22% (http://landsat.usgs.gov/products_slcoffbackground.php). Most selected plots were

located in the center of the image and thus not affected by the data loss, e.g. the forest plots located at the edges of the scan line error zone faced minimal data loss because they were large enough.

We also downloaded the tile h28v09 of the MODIS Terra (MOD) and Aqua (MYD) daily 1km Land Surface Temperature and Emissivity products (MOD11A1 and MYD11A1 Collection-5) and MODIS 16-days 500 m Vegetation Indices NDVI/EVI product (MOD13A1 Collection-5) from 05 March 2000 till 31 December 2015 for Terra data and from 8 July 2002 till 31 December 2015 for Aqua data. We downloaded other supporting satellite data such as the MODIS Atmospheric Profile product (MOD07_L2) and the MODIS Geolocation product (MOD03). All MODIS data were reprojected to WGS84, UTM zone 48 South with the MODIS Reprojection Tool (MRT). The quality of the MODIS data was examined with the provided quality flags and only pixels with the highest quality flag were used in the analysis.

2.4 Retrieval of biophysical variables from Landsat 7 ETM+ VIS/TIR images

- *NDVI*

NDVI was derived from the reflectances corrected for atmospheric effects in the red (ρRED, band 3 Landsat 7 ETM+) and near infrared (ρNIR, band 4 Landsat 7 ETM+) bands, with:

$$NDVI = \frac{\rho NIR - \rho RED}{\rho NIR + \rho RED} \quad (1)$$

- *Surface albedo*

The surface albedo (α) was computed with the equation of Liang (2000) for estimating broadband albedo from Landsat surface reflectance bands, with:

$$\alpha = 0.3141\ \rho_1 + 0.1607\ \rho_3 + 0.369\ \rho_4 + 0.1160\ \rho_5 + 0.0456\ \rho_7 - 0.0057 \quad (2)$$

where ρ_1, ρ_3, ρ_4, ρ_5 and ρ_7 are the Landsat 7 ETM+ surface reflectance bands (corrected for atmospheric effects).

- *Surface temperature (LST)*

LST was derived following the method proposed by Bastiaanssen (2000), Bastiaanssen et al. (1998a), Coll et al. (2010) and Wukelic et al. (1989) for computing the surface temperature from the thermal infrared band (TIR, band 6) of Landsat (Supporting information, S1). The thermal infrared band (TIR, band 6) was first converted to thermal radiance (L6, W/m^2/sr/µm) and then to atmospherically corrected thermal radiance (Rc, W/m^2/sr/µm) as described by Wukelic et al. (1989) and Coll et al. (2010), and with the atmospheric parameters obtained on NASA's online Atmospheric Correction Calculator (Barsi et al., 2003, 2005) (supporting information, S2). The surface temperature (LST, K) was computed with the following equation similar to the Planck equation, as in Coll et al. (2010) and Wukelic et al. (1989):

$$\mathrm{LST} = \frac{\mathrm{k2}}{\ln\left(\frac{\varepsilon\mathrm{NB}\cdot\mathrm{k1}}{\mathrm{Rc}}+1\right)} \quad (3)$$

where εNB is the emissivity of the surface obtained from the NDVI (Supporting information, Table S1), k1 (= 666.09 mW/cm^2/sr/µm) and k2 (= 1282.71 K) are sensor constants for converting the thermal radiance obtained from band 6 of Landsat 7 to surface temperature.

299 The surface temperature derived from Landsat thermal band was compared with the MODIS
300 LST product that was acquired on the same day at 10:30 am local time. The Landsat LST image
301 was first resampled to MODIS resolution to enable a pixel to pixel comparison, followed by
302 extracting the average LST of 7 land cover types with the data set containing the large
303 delineated plots (Fig. 1).
304
305 • *Evapotranspiration (ET)*
306
307 Based on the Surface Energy Balance Algorithm for Land (SEBAL) (Bastiaanssen, 2000;
308 Bastiaanssen et al., 1998a, 1998b) we estimated ET (mm/hr) from latent heat fluxes (LE, W/m^2)
309 which were computed as the residual from sensible (H, W/m^2) and ground (G, W/m^2) heat
310 fluxes subtracted from net radiation (Rn, W/m^2) as:
311
312 $$LE = Rn - G - H \quad (4)$$
313
314 We calculated Rn as the sum of incoming shortwave and longwave radiation, minus the
315 reflected shortwave and longwave radiation and the emitted longwave radiation (equation 5).
316 The surface albedo, surface emissivity and surface temperature determine the amounts of
317 incoming and reflected radiation:
318
319 $$Rn = (1 - \alpha)\, S_d\downarrow + \varepsilon_a \sigma T_a^4 - (1 - \varepsilon_0)\varepsilon_a \sigma T_a^4 - \varepsilon_0 \sigma LST^4 \quad (5)$$
320
321 Where $S_d\downarrow$ is the incoming shortwave solar radiation (W/m^2) at the surface; α is the surface
322 albedo (equation 2); ε_0 is the surface emissivity (-); ε_a is the atmospheric emissivity (-); σ is the
323 Stephan-Boltzmann constant (5.67×10^{-8} $W/m^2/K^4$); LST is the surface temperature (K,
324 equation 3); T_a is the sky temperature (K). The surface emissivity (ε_0) is derived from the NDVI

and is described in the supporting information (Table S1). The average atmospheric emissivity (ε_a) is estimated with the model of Idso and Jackson, (1969):

$$\varepsilon_a = 1 - 0.26 \times \exp\left((-7.77 \times 10^{-4}) \times (273.15 - T_a)^2\right) \quad (6)$$

Ground heat fluxes (G, W/m^2) were derived as a fraction of Rn from an empirical relationship between LST, α, and NDVI (Bastiaanssen, 2000) as:

$$G = Rn \times \frac{LST - 273.15}{\alpha} \times (0.0038\alpha + 0.0074\alpha^2) \times (1 - 0.98NDVI^4) \quad (7)$$

In SEBAL Sensible heat flux (H, W/m^2) was calculated as:

$$H = \rho Cp \frac{\Delta T}{r_{ah}} = \rho Cp \frac{a\,LST + b}{r_{ah}} \quad (8)$$

Where ρ is the air density (1.16 kg/m^3); Cp is the specific heat of air at constant pressure (1004 J/kg/K); r_{ah} is the aerodynamic resistance to heat transport (s m^{-1}); *a* and *b* are regression coefficients which are determined by a hot extreme pixel (where LE = 0 and H is maximum) and a cold extreme pixel (where H = 0 and LE is maximum). The aerodynamic resistance to heat transport, r_{ah}, is calculated through an iterative process with air temperature measured at 2 m as input. SEBAL is described in Bastiaanssen (2000) and Bastiaanssen et al. (1998a, 1998b). The application of SEBAL in this research is briefly described in the supporting information (S3: ET from satellite images).

2.5 Local short term differences between different land cover types

From the created LST, NDVI, Albedo and ET images we extracted the average values of the different land cover classes with the data set containing the small 49 delineated plots covering 7 different land cover types (Fig. 1). The average effect of land transformation, i.e. the change from forest to another non-forest land cover type, on the surface temperature was evaluated as (cf. Li et al. (2015)) :

$$\Delta LST = LST_{non\text{-}forest} - LST_{forest} \quad (9)$$

A negative ΔLST indicates a cooling effect and positive ΔLST indicates a warming effect of the non-forest vegetation compared with forest. The same procedure was applied in evaluating the effect of land transformation on the NDVI, albedo and ET.

2.6 Effects of land cover change on the provincial surface temperature in the past decades

To analyse the long-term effects on the provincial scale we used the MODIS daily LST time series (MOD11A1 and MYD11A1) from 2000 – 2015. MOD11A1 provides LST for 10:30 am and 10:30 pm and we used the times series between 2000 and 2015. MYD11A1 provides LST for 1:30 am and 1:30 pm and is available from 8 July 2002; we used complete years in our analysis and therefore used the MYD11A1 time series from 2003 – 2015. We calculated the mean annual LST at four different times of the day (10:30 am, 1:30 pm, 10:30 pm and 1:30 am) between 2000 and 2015 for the lowland of Jambi from the MODIS daily LST time series (MOD11A1 and MYD11A1). First, (1) we calculated for each pixel the average LST pixel value using only the best quality pixels for every year; (2) from these pixels we made a composite image (n = 16, one for each year) for the province and (3) from each composite image we calculated the mean annual lowland provincial temperature as the average of all the pixels that are enclosed by a zone delineating the lowland of the Jambi province. We performed

376 the same analysis with the MODIS 16-day NDVI product (2000 – 2015) and the ERA daily
377 temperature grid (2000 – 2015) to compare the annual trends of LST, NDVI and air temperature
378 of the province. The average provincial LST and NDVI were compared with the mean LST and
379 NDVI of a selected forest that remained undisturbed forest during the 2000 – 2015 period.
380
381 **2.7 Statistical analysis**
382
383 For a comparison of the Landsat derived LST and the MODIS LST we analyzed the statistical
384 relationships with the coefficient of determination (R^2), the root mean square error (RMSE),
385 the mean absolute error (MAE) and the bias (Bias):
386
387 $$\text{RMSE} = \sqrt{\frac{\sum_{i=1}^{N}(E_i - O_i)^2}{N}} \quad (10)$$
388
389 $$\text{Bias} = \frac{\sum_{i=1}^{N}(E_i - O_i)}{N} \quad (11)$$
390
391 $$\text{MAE} = \frac{\sum_{i=1}^{N}|E_i - O_i|}{N} \quad (12)$$
392
393 Where O_i is MODIS LST, E_i is the Landsat surface temperature, and N is the number of pixels
394 compared. Model type 2 linear regression was applied for fitting the relation between MODIS
395 LST and Landsat LST.
396 We tested the relation between the biophysical variables LST (or L6 and Rc, both as pre- or
397 intermediate products before obtaining LST), albedo (α), NDVI and ET with a correlation
398 analysis and a multiple linear regression was applied to analyse the effects of the biophysical
399 variables on the LST. We used the model: LST (or Rc or L6) ~ α + NDVI + ET, and used R^2

and standardized β-coefficients to evaluate the strength of the biophysical variables in predicting the LST.

3 Results

3.1 Landsat LST compared to MODIS LST

Landsat and MODIS images showed similar spatial LST patterns (Fig. 2). In both images the relatively hot areas (red) correspond to the known clear cut areas, urban areas or other sparsely vegetated areas, the relatively cool areas (blue) correspond to vegetated areas such as forest, plantation forests and mature oil palm plantations. The coarse resolution scale of MODIS (1000 m for LST) allows a large regional coverage of the study area but does not allow to retrieve detailed information on small patches (smaller than 1 km^2). On the other hand, the Landsat 7 image allows a detailed study of patches that are small enough (as small as 30 x 30 m^2), but is affected by the scan line error causing data loss at the edges of the image. In both MODIS and Landsat images clouds and cloud shadows were removed and therefore lead to data gaps in the images.

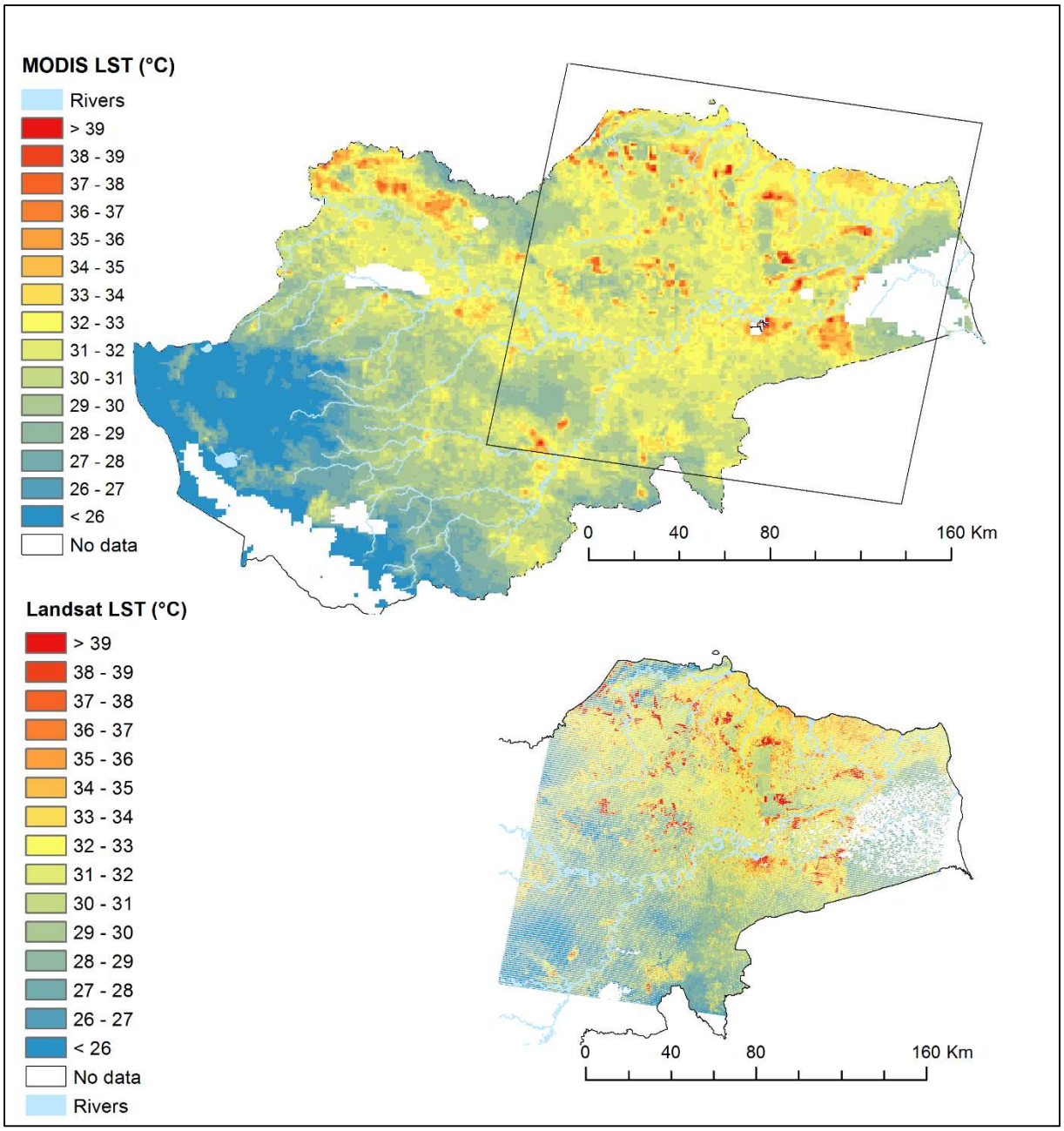

Fig. 2 MODIS LST image (top) compared with Landsat LST image (bottom). Cloud cover and cloud shadow cover resulted in data gaps (No data). The difference in acquisition time between the images is 15 minutes. The square in the MODIS image is the area that is covered by the Landsat tile (path 125, row 61). Both satellite images were acquired on 19 June 2013.

Landsat derived LST correlated well with MODIS LST ($R^2 = 0.82$; $p < 0.001$; Fig. 3) with a RMSE of 1.8 ºC. The 7 land cover types had distinctive LSTs and the observed differences

between these land cover types were consistent in both images. The non-vegetated surfaces (Clear cut land (CLC) and Urban areas (UB)) had higher surface temperatures than the vegetated surface types (FO, YOP, MOP, PF and RU). Clear cut land had the highest surface temperature of all compared land cover types, followed by urban areas whereas the vegetated land cover types had lower surface temperatures: LST_{CLC} (39.7 ± 2.0 °C) > LST_{UB} (35.8 ± 1.3 °C) > LST_{YOP} (31.0 ± 0.7 °C) > LST_{PF} (30.3 ± 0.7 °C) > LST_{MOP} (29.0 ± 0.8 °C) > LST_{RU} (27.8 ± 0.9 °C) > LST_{FO} (27.6 ± 1.4 °C) (Landsat LST, Fig. 3). The same trend was derived from the MODIS image but with higher surface temperatures, except for CLC: LST_{CLC} (37.7 ± 1.8 ºC) > LST_{UB} (36.3 ± 1.6 °C) > LST_{YOP} (31.7 ± 0.9 ºC) > LST_{MOP} (30.7 ± 0.9 ºC) > LST_{PF} (29.9 ± 0.9 ºC) > LST_{RU} (29.6 ± 0.4 ºC) > LST_{FO} (29.2 ± 0.4 ºC) (MODIS LST, Fig. 3).

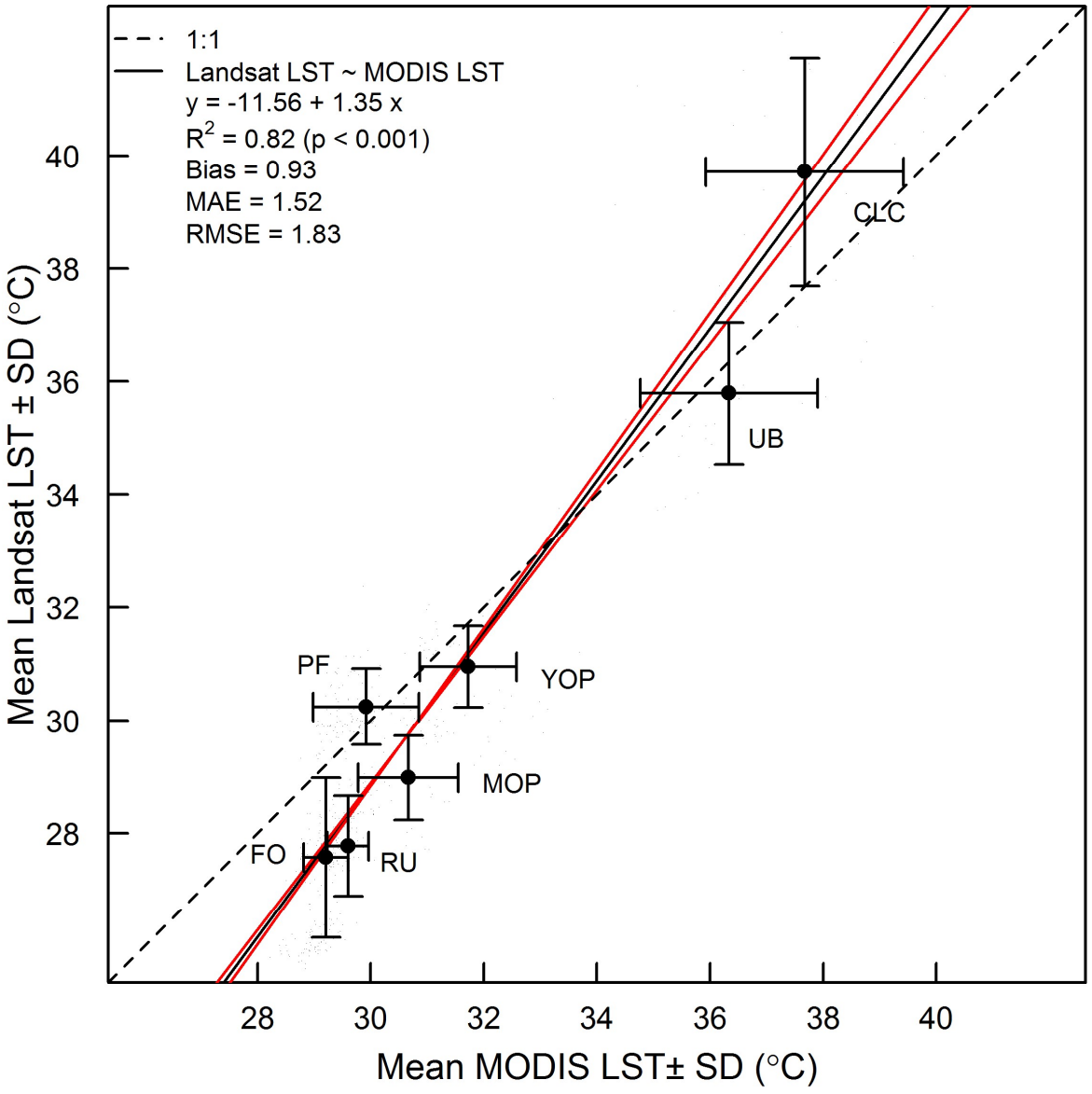

Fig. 3 Average surface temperature (LST) and standard deviation (SD) of 7 land cover types derived from a Landsat thermal image compared with the mean and SD of MODIS LST. CLC = Clear cut land, UB = Urban areas, YOP = young oil palm plantation, PF = Acacia Plantation Forest, MOP = Mature Oil palm plantation, FO = Forest, RU = Rubber plantation. The dashed line is the theoretical 1:1 line, the solid lines are the Linear Model type 2 regression line (black) and the confidence limits of the regression line (red). The Landsat and MODIS images were acquired on 19 June 2013, at 10:13 am and 10:30 am local time respectively. Landsat pixels (30 m) were resampled to MODIS pixel resolution (926 m) to make a pixel to

449 pixel comparison between the two sources possible. RMSE is the root mean squared error, MAE
450 is the mean absolute error.
451
452 **3.2 Local short term differences between different land cover types**
453
454 The ΔLST between RU, MOP, PF, YOP, UB and CLC land cover types and FO were all
455 positive, meaning that the other land cover types were warmer than forests (Fig. 4a &
456 Supporting Information S4 and S5). RU and MOP were 0.4 ± 1.5 °C and 0.8 ± 1.2 °C warmer
457 than forest, respectively. PF and YOP were much warmer than forests (ΔLST_{PF-FO} = 2.3 ± 1.1
458 °C, ΔLST_{YOP-FO} = 6.0 ± 1.9 °C). The largest ΔLSTs were between forest and the non-vegetated
459 land cover types, i.e. UB (ΔLST = 8.5 ± 2.1 °C) and CLC (ΔLST = 10.9 ± 2.6 °C). The LST
460 differences were significant ($p < 0.05$, post-hoc Tukey's HSD test), except between RU and FO
461 ($p = 0.78$, post-hoc Tukey's HSD test (Supporting Information S6, Table S6.1 & table S6.2).
462
463 Similar differences were found for the ΔNDVI between forest and the other land covers (Fig.
464 4b). The negative ΔNDVI indicates that the non-forest land cover types had lower NDVI than
465 forest. ΔNDVI between FO and RU, MOP, PF and YOP were small (between – 0.01 ± 0.02
466 ($\Delta NDVI_{MOP-FO}$) and – 0.12 ± 0.06 ($\Delta NDVI_{YOP-FO}$). The largest ΔNDVIs were between forest
467 and the non-vegetated land cover types, i.e. UB and CLC (ΔNDVI = – 0.42 ± 0.11 and – 0.41
468 ± 0.08, respectively). All ΔNDVIs were significant ($p < 0.05$, post-hoc Tukey's HSD test).
469
470 The difference in albedo (ΔAlbedo) between forest and the other land covers was very small
471 (Fig. 4c), with ΔAlbedo values between – 0.03 ± 0.01 ($\Delta Albedo_{PF-FO}$) and 0.03 ± 0.02
472 ($\Delta Albedo_{YOP-FO}$). These differences were significant ($p < 0.05$, post-hoc Tukey's HSD test).
473 PF had a lower albedo than forest ($\Delta Albedo_{PF-FO}$ = – 0.03 ± 0.01), while the other land cover
474 types had a higher albedo than forest.

All compared land covers had lower ET than forest. RU, MOP and PF had slightly lower ET than FO ($\Delta ET_{RU-FO} = -0.03 \pm 0.04$, $\Delta ET_{MOP-FO} = -0.03 \pm 0.03$ mm/hr, $\Delta ET_{PF-FO} = -0.04 \pm 0.03$ mm/hr) (Fig. 4d). YOP, UB and CLC had much lower ET values than forests: $\Delta ET_{YOP-FO} = -0.18 \pm 0.04$ mm/hr, $\Delta ET_{UB-FO} = -0.23 \pm 0.04$ mm/hr, $\Delta ET_{CLC-FO} = -0.26 \pm 0.06$ mm/hr). The ΔETs were significant ($p < 0.05$, post-hoc Tukey's HSD test). The SEBAL based LE estimates were within the variability range of LE measurements from eddy covariance measurements under similar meteorological conditions (see SI 3).

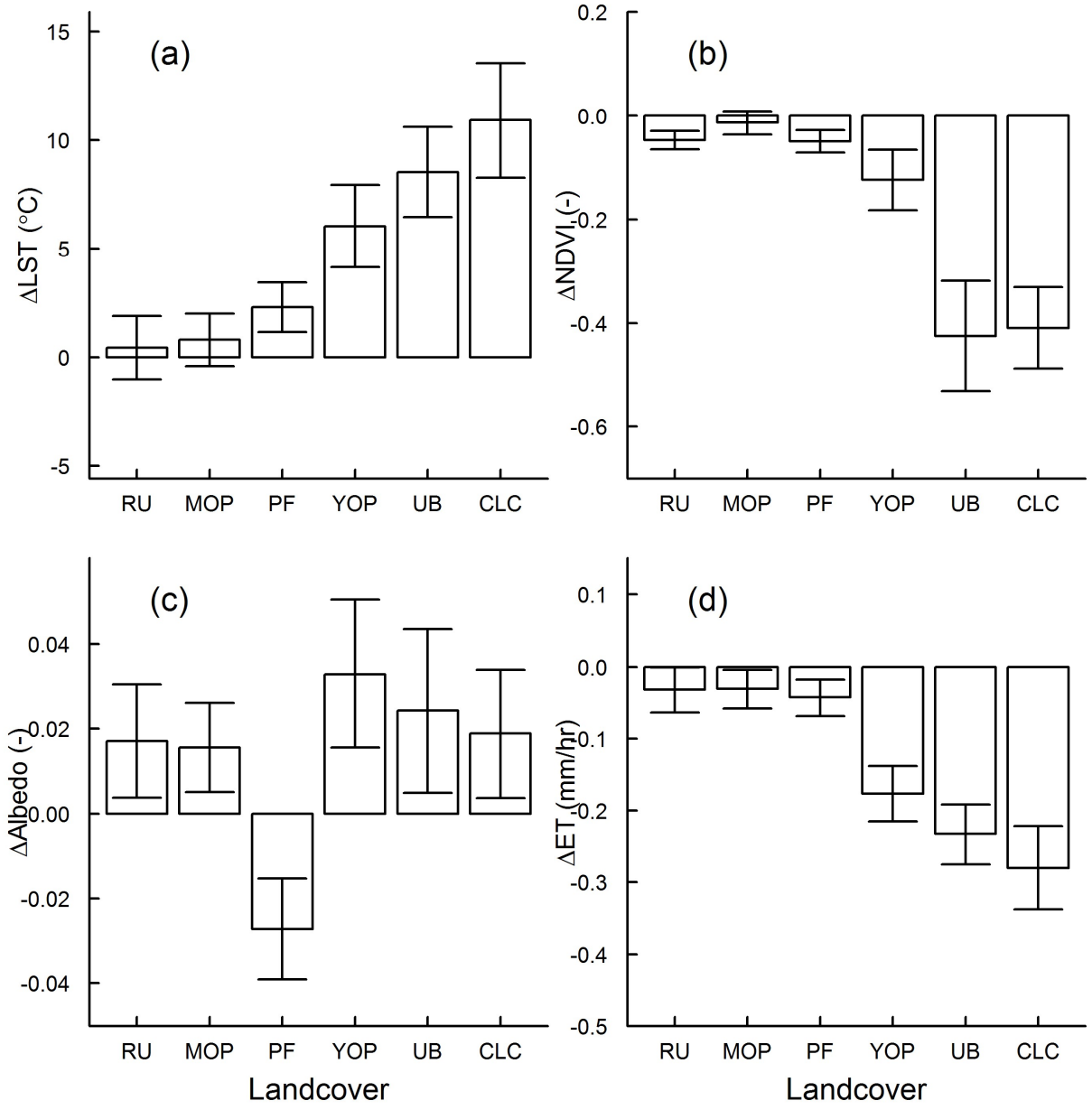

Fig. 4 Differences (mean ± SD) in surface temperature (ΔLST), normalized difference vegetation index (ΔNDVI), Albedo (ΔAlbedo) and Evapotranspiration (ΔET) between other land covers (RU, MOP, PF, YOP, UB and CLC) and forest (FO) in the Jambi province, derived from a Landsat LST image acquired on 19 June 2013 at 10:13 am local time.

Albedo had a weaker influence on the LST ($\rho = 0.25$, $p < 0.05$) (Table 2) than NDVI and ET. As the thermal radiance band (L6) and the atmospherically corrected thermal band (Rc) were the basis for the LST calculation, the high correlation between L6 and NDVI ($\rho = -0.87$, $p <$

493 0.05) and between L6 and ET ($\rho = -0.98$, $p < 0.05$) resulted in a high correlation between LST
494 and NDVI ($\rho = -0.88$) and between LST and ET ($\rho = -0.98$). The analysis showed that albedo,
495 NDVI and ET were all significant predictors of LST ($F_{(3, 41586)} = 1 \times 10^6$, $p < 0.05$). ET was the
496 strongest predictor of LST (stand. $\beta = -1.11$, $p < 0.05$). Albedo (stand. $\beta = -0.19$, $p < 0.05$)
497 and NDVI (stand. $\beta = -0.19$, $p < 0.05$) were weaker predictors of LST.
498
499 **Table 2** Statistical analysis between biophysical variables (albedo (α), NDVI and ET) and
500 Spectral Radiance band (L6), corrected thermal band (Rc) and Landsat surface temperature
501 (LST).

Model		ρ	R^2	β	Stand. β	Model fit (R^2)	F-statistics
L6 ~ α + NDVI + ET	**α**	0.26	0.05	-2.94	-0.19	0.99	F (3, 41586) = 1.10×106, ***
	NDVI	-0.87	0.10	0.23	0.11		
	ET	-0.98	1.13	-4.00	-1.16		
Rc ~ α + NDVI + ET	**α**	0.25	0.05	-4.88	-0.20	0.99	F (3, 41586) = 1.79×106 , ***
	NDVI	-0.88	0.04	0.16	0.05		
	ET	-0.98	1.00	-6.21	-1.10		
LST ~ α + NDVI + ET	**α**	0.25	0.05	-34.01	-0.19	0.99	F(3, 41586) = 2.3×106, ***
	NDVI	-0.88	0.05	1.30	0.05		
	ET	-0.98	1.00	-43.53	-1.11		

502 ***: $p = 2\times10^{-16}$
503 LM: Multiple linear regression analysis between LST (or L6 or Rc) and 3 biophysical variables:
504 Albedo (α), NDVI and ET. ρ = correlation coefficient; R^2: R-squared of the components; β =
505 regression coefficient of the component; stand. β = standardized β; Model fit (R^2): overall model
506 fit of the multiple linear regression.
507
508 A separate analysis (Table S6.3, Supporting information S6) showed that ET was a strong
509 predictor of LST for each land cover type in this study and that NDVI and albedo were minor
510 predictors of LST.
511

3.3 Effects of land-use change on the provincial surface temperature in the past decades

The average annual LST of Jambi was characterized by a fluctuating but increasing trend during daytimes (Fig. 5a and 5b) between 2000 and 2015. The average morning LST (10:30 am) increased by 0.07 ºC per year ($R^2 = 0.59$; $p < 0.001$), the midday afternoon LST (13:30 local time) increased by 0.13 °C per year ($R^2 = 0.35$; $p = 0.02$) between 2003 and 2015. While the daytime LST showed a clear increase, the night and evening LST (10:30 pm and 1:30 am, Fig. 5c and 5d) trends showed a small decrease of – 0.02 °C ($R^2 = 0.29$; $p = 0.02$) and – 0.01 °C ($R^2 = 0.05$; $p = 0.50$) per year, respectively. The observed LST trends resulted in a total LST increase of 1.05 °C and 1.56 °C in the morning (10:30 am) and afternoon (1:30 pm) respectively and a total decrease of the LST of 0.3 °C (10:30 pm) and 0.12 °C (1:30 am) at night over the period from 2000 to 2015 in Jambi.

To separate the effect of land use change from global climate warming, we used a site constantly covered by forest over that period (from the forest sites we used in this study) as a reference that was not directly affected by land cover changes. That site showed smallchanges in LST than the entire province: only the mean morning LST (10:30 am) had a significant but small trend with an increase of 0.03 °C per year ($R^2 = 0.21$, $p < 0.05$) resulting in a total LST increase of 0.45 °C between 2000 and 2015 (Fig. 5a). This LST warming is much smaller than the overall warming at provincial level of 1.05 °C. The LST time series at other times showed no significant trends: the mean afternoon LST (1:30 pm) increased by -0.05 °C per year ($R^2 = 0.01$, $p = 0.31$) (Fig. 5b), the night and evening LST by 0.01°C per year (Fig. 5c and 5d, $p = 0.19$ and $p = 0.60$, respectively).

536 The mean annual NDVI in Jambi decreased by 0.002 per year, resultingin a total NDVI decrease
537 of 0.03 (R^2 = 0.34; p = 0.01; Fig. 5e). The NDVI of the forest showed a small but not significant
538 increase of 0.001 per year (R^2 = 0.04, p = 0.23) (Fig. 5e) fluctuating around an NDVI of 0.84.
539
540 The mean annual midday air temperature (at 1:00 pm, local time, Fig. 5f) and the mean annual
541 night air temperature (at 1:00 am, local time) increased every year by 0.05 °C and 0.03 °C
542 respectively, resulting in a total air temperature increase of 0.75 °C (R^2 = 0.66, p < 0.001) and
543 0.45 °C (R^2 = 0.32, p = 0.01) between 2000 and 2015 (Fig. 5f).

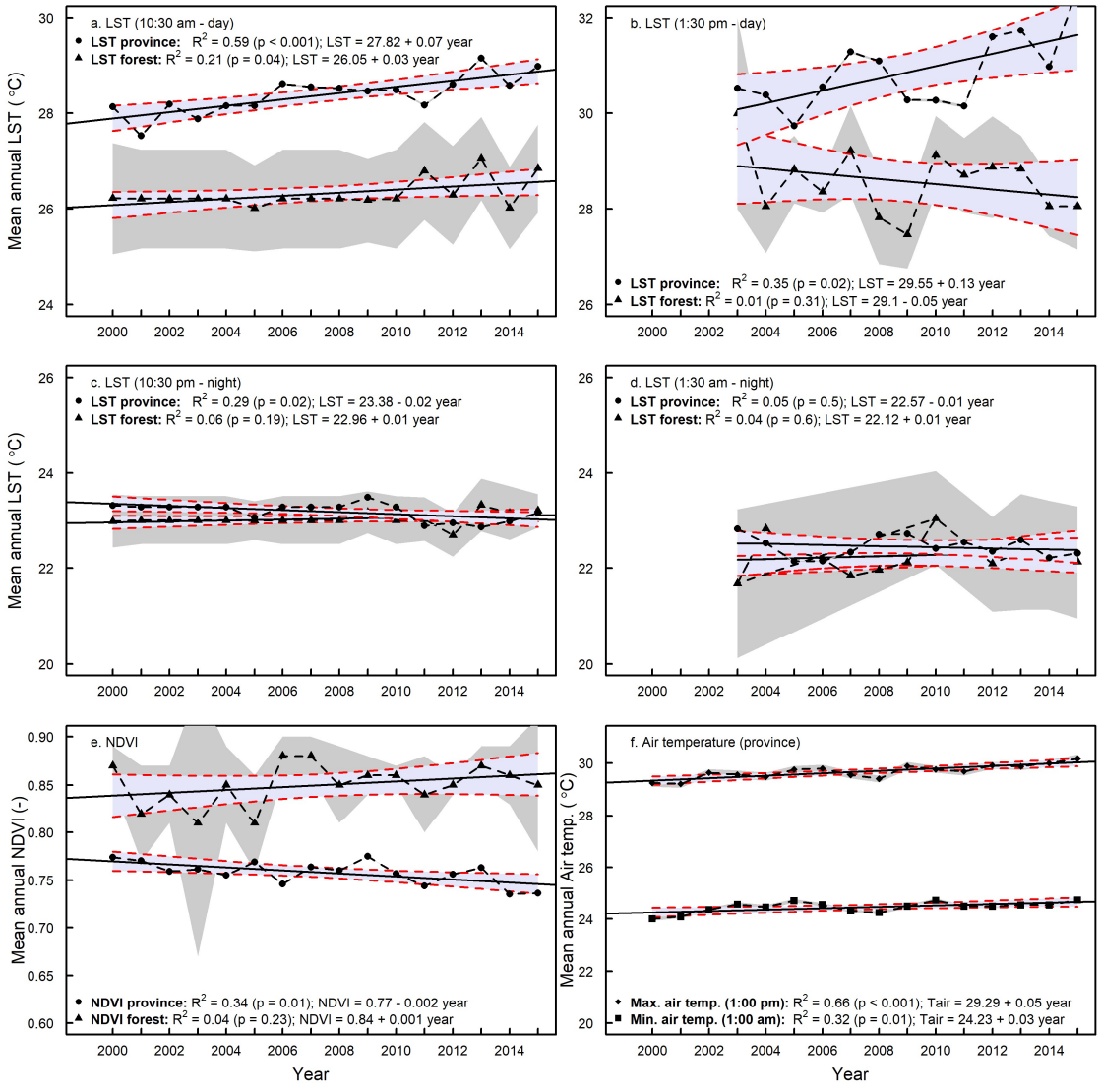

544
545 **Fig 5**. Mean annual LST (a – d), mean annual NDVI (e) and mean annual air temperature trends
546 (f) in the Jambi province between 2000 and 2015 derived from MODIS LST (5a. 10:30 am, 5b.

1:30 pm, 5c. 10:30 pm and 5d. 1:30 am, local time), MODIS NDVI and ERA Interim Daily air temperature (1:00 am and 1:00 pm, local time) data sets respectively. Grey-shaded areas are the confidence intervals of the means, blue-shaded areas are the confidence intervals of the regression lines. MODIS LST time series for 1:30 pm and 1:30 am were available from the mid of 2002; for this reason we used the complete years from 2003 till 2015.

4 Discussion

4.1 Landsat LST compared to MODIS LST

In our study we retrieved the surface temperature from a Landsat image and compared this with MODIS LST. Our results showed a good agreement between both LSTs (Fig. 3), which is comparable to other studies and thus gives confidence in our analysis. Bindhu et al. (2013) found also a close relationship between MODIS LST and Landsat LST by using the same aggregation resampling technique as our method and found a R^2 of 0.90, a slope of 0.90, and an intercept of 25.8 °C for LST, compared to our R^2 of 0.8, slope of 1.35 and intercept of –11.58 °C (Fig. 3). Zhang and He (2013) validated Landsat LST with MODIS LST and also found good agreements (RMSD 0.71 – 1.87 ºC) between the two sensors, whereas we found a RMSE of 1.71 ºC. Nevertheless, there still are differences and slope versatility between the two satellite sources. These differences are typically caused by differences between the MODIS and Landsat sensors in terms of (a) different sensor properties e.g. spatial and radiometric resolution and sensor calibration; (b) geo-referencing and differences in atmospheric corrections (Li et al., 2004); and (c) emissivity corrections i.e. the use of approximate equations to derive the emissivity from the NDVI from Landsat's Red and NIR bands. Li et al. (2004) and Vlassova et al. (2014) identified these same factors in their comparison of ASTER LST with MODIS LST and Landsat LST with MODIS LST, respectively. Vlassova et al. (2014) found good

agreements between MODIS and Landsat LST and obtained higher LSTs with MODIS than with Landsat, which they attributed to the delay of 15 minutes in acquisition time between MODIS and Landsat. MODIS LST is measured 15 minutes later and our results showed that MODIS LSTs were indeed higher than Landsat LST. A comparison of MODIS LST with locally measured canopy surface temperatures during the overpass time of MODIS also showed agreement (Supporting information S7, Figure S7.1). The slope was possibly related to differences in instrumentation and emissivity corrections and to scale issues, still this comparison could corroborate the quality check of MODIS LST.

As the MODIS LST product is proven to be accurate within 1 ºC (Silvério et al., 2015; Wan et al., 2004) and has been intensively validated, the use of MODIS LST was a proper way to assess the quality of our Landsat LST.

The errors from the different sources (such as atmospheric correction, emissivity correction, resampling Landsat to MODIS resolution) are difficult to quantify. When we tested the impact of atmospheric correction and emissivity errors on the LST from Landsat retrieval we found that: (a) the overall patterns across different land use types did not change, (b) emissivity was the most important factor, but the effects on LST retrieval were small and (c) errors related to atmospheric correction parameters were small because there were minor differences between the default atmospheric correction (ATCOR) parameters and the ATCOR parameters derived with actual local conditions (relative humidity (RH), air pressure and air temperature). Following the method of Coll et al. (2009) and Jiang et al. (2015) we show that the use of the online atmospheric correction parameter calculator is a good option provided that RH, air temperature and air pressure measurements are available. We additionally compared locally measured air temperatures with MODIS air temperature and found a good agreement (Supporting information S8, Figure S8.1), which served as a verification that we used a correct air temperature for the atmospheric correction parameter calculator.

599 Overall, our comparison of Landsat LST with MODIS LST and against ground observations
600 suggests that we are able to retrieve meaningful spatial and temporal patterns of LST in the
601 Jambi province.
602
603 **4.2 LST patterns across different land use and land cover (LULC) types**
604
605 The land cover types in our study covered a range of land surface types that develop after forest
606 conversion. This is the first study in this region that includes oil palm and rubber as land use
607 types that develop after forest conversion. The coolest temperatures were at the vegetated land
608 cover types while the warmest surface temperatures were on the non-vegetated surface types
609 like urban areas and bare land. Interestingly, the oil palm and rubber plantations were only
610 slightly warmer than the forests whereas the young oil palm plantations had clearly higher LST
611 than the other vegetated surfaces. For other parts of the world, Lim et al. (2005, 2008), Fall et
612 al. (2010) and Weng et al. (2004) also observed cooler temperatures for forests and the highest
613 surface temperatures for barren and urban areas.
614 In Indonesia, land transformation is often not instantaneous from forest to oil palm or rubber
615 plantation, but can be associated with several years of bare or abandoned land in-between (Sheil
616 et al., 2009). Oil palm plantations typically have a rotation cycle of 25 years, resulting in
617 repeating patterns with young plantations (Dislich et al., 2016). Given the large LST differences
618 between forests and bare soils or young oil palm plantations that we observed, a substantial
619 warming effect of land transformation at regional scale is expected.
620
621 **4.3 Drivers of local differences between different land cover types**
622
623 All the land cover types (except Acacia Plantation Forests) had a higher albedo than forest,
624 indicating that these land cover types absorbed less incoming solar radiation than forests.

Nevertheless, these land cover types were warmer than forests, suggesting that the albedo was not the dominant variable explaining the LST. Indeed, the statistical analysis showed that ET ~ LST had a higher correlation than albedo ~ LST. The ΔETs were significant, underlying that despite their higher albedo, all land cover types had higher LSTs than forests related to lower ET rates than forests. On the other hand, forests that absorb more solar radiation because of the lower albedo, have lower LST because of the higher ET they exhibit, hereby identifying evaporative cooling as the main determinant of regulating the surface temperature of all vegetation cover types (Li et al., 2015).

Both observational and modeling studies carried out in other geographic regions and with other trajectories support our observations. Observational studies in the Amazonia by Lawrence and Vandecar (2015) on the conversion of natural vegetation to crop or pasture land showed a surface warming effect. Salazar et al. (2015) provided additional evidence that conversion of forest to other types of land use in the Amazonia caused significant reductions in precipitation and increases in surface temperatures.

Alkama and Cescatti (2016) and earlier studies by Loarie et al. (2011a, 2011b) showed that tropical deforestation may increase the LST. Croplands in the Amazonian regions were also warmer than forests through the reduction of ET (Ban-Weiss et al., 2011; Feddema et al., 2005) and that the climatic response strongly depends on changes in energy fluxes rather than on albedo changes (Loarie et al., 2011a, 2011b). A study by Silvério et al. (2015) indeed found that tropical deforestation changes the surface energy balance and water cycle and that the magnitude of the change strongly depends on the land uses that follow deforestation. They found that the LST was 6.4 ºC higher over croplands and 4.3 ºC higher over pasture lands compared to the forest they replaced, as a consequence of energy balance shifts. Ban-Weiss et al. (2011) and Davin and de Noblet-Ducoudré (2010) added that in addition to the reduction of ET, the reduction of surface roughness most likely enhanced the substantial local warming.

Also for non-Amazonian regions, the replacement of forests by crops caused changes comparable with our observations. In temperate Argentina, Houspanossian et al. (2013) found that the replacement of dry forests by crops resulted in an increase of albedo but still forests exhibited cooler canopies than croplands. The cooler canopies were a result of a higher aerodynamic conductance that enhanced the capacity of tree canopies to dissipate heat into the atmosphere, and to both latent and sensible heat fluxes operating simultaneously to cool forest canopies.

In a global analysis Li et al. (2015) showed that tropical forests generally have a low albedo, but still the net energy gain caused by solar energy absorption is offset by a greater latent heat loss via higher ET and that in the tropical forests the high ET cooling completely offsets the albedo warming. For China, this cooling effect was also shown by Peng et al. (2014) who compared LST, albedo and ET of plantation forests, grassland and cropland with forests.

For the USA, Weng et al. (2004) and for China, Yue et al. (2007), using NDVI as an indicator of vegetation abundance, also found that areas with a high mean NDVI had a lower LST than areas with a low mean NDVI, therefore suggesting that vegetation abundance is an important factor in controlling the LST through higher ET rates. Our result support their assumptions by showing the high correlation between NDVI – LST and ET – LST.

Our findings are also supported by modelling studies. Beltrán-Przekurat et al. (2012) found for the Southern Amazon that conversion of wooded vegetation to soy bean plantations caused an increase of the LST due to decreased latent heat and increased sensible heat fluxes. Climate models also show the same warming trends and land surface modelling also projects an increase in surface temperatures following deforestation in the Brazilian Cerrado (Beltrán-Przekurat et

al., 2012; Loarie et al., 2011b). In a global analysis, Pongratz et al. (2006) showed a LST increase of forest to cropland or pasture transitions, which was driven by a reduced roughness length and an increased aerodynamic resistance, and that the temperature response is intensified in forest to clear/bare land transitions (1.2 – 1.7 ºC increase). Similar to observational studies, the modelling results of Bathiany et al. (2010) show that ET is the main driver of temperature changes in tropical land areas.

To understand the effects of deforestation on biophysical variables in Indonesia, our study identifies the following mechanisms: (a) reduction of ET decreases surface cooling, (b) reduced surface roughness reduces air mixing in the surface layer and thus vertical heat fluxes, (c) changes in albedo change the net radiation, and (d) changes in energy partitioning in sensible and latent heat and heat storage. The effect is an increase of the mean temperatures leading to warming effects in all tropical climatic zones (Alkama and Cescatti, 2016). We point here that our study (1) included a ground heat flux, but did not take into account the storage of heat in the soil and the release of stored heat out of the soil during the daily cycle and (2) that the Landsat satellite image was obtained under cloud free conditions with high shortwave radiation input and low fraction of diffuse radiation. Therefore, the LST retrieved on cloud free days might be overestimated compared to cloudy days, as the differences in LST between land uses are supposed to be lower when diffuse radiation increases.

Our study is the first to include the oil palm and rubber expansion in Indonesia. In Indonesia, smallholders take 40% of the land under oil palm cultivation for their account (Dislich et al., 2016). Because the landscape in Jambi is characterized by a small-scale smallholder-dominated mosaic including rubber and oil palm monocultures (Clough et al., 2016), studies using medium to coarse resolution data are not able to capture the small scale changes and processes at the small-scale level. By using high resolution Landsat data we were also able to include the effects

of land use change on biophysical variables and the underlying processes of the small scale holder agriculture.

4.4 Effects of land use change on the provincial surface temperature in the past decades

The increases of the mean surface temperature in Jambi were stronger during the morning (10:30 am) and afternoon (1:30 pm) than during the evening (10:30 pm) and night (1:30 am). Given that our results show a decrease of the NDVI in the same period, this suggests that the observed increased trend of the day time LST can be attributed to the land cover changes that occurred. Our assumption that the observed decreasing NDVI trend is caused by land conversions is supported by two different studies which reported that in Jambi, between 2000 and 2011 (Drescher et al., 2016) and between 2000 and 2013 (Clough et al., 2016), the forest area decreased and that the largest increases were for rubber, oil palm, and agricultural and tree crop areas. The class 'other land use types', which includes urban areas, showed a minor increase (around 1%), suggesting that the decrease in NDVI was most likely caused by forest cover loss and not by urban expansion (see Supporting information, Table S9). The same observations on LULC change in Indonesia were also done by Lee et al. (2011), Margono et al. (2012, 2014) and Luskin et al. (2014). Luskin et al. (2014) showed that in Jambi, during the period 2000 – 2010, forests decreased by 17% while oil palm and rubber area increased by 85% and 19%, respectively.

Given these trends in LULC changes, the observed LST trends were most likely caused by gradual decrease of forest cover loss at the expense of agriculture and croplands. Our assumptions are supported by findings of Silvério et al. (2015), Costa et al. (2007), Oliveira et al. (2013), Spracklen et al. (2012) and Salazar et al. (2015) which indicate that land use transitions in deforested areas likely have a strong influence on regional climate. Alkama and

729 Cescatti (2016) show that biophysical effects of forest cover changes can substantially affect
730 the local climate by altering the average temperature, which is consistent with our observations
731 and can be related to the observed land use change in the Jambi province. As Indonesia has
732 undergone high rates of forest cover loss from 2000 to 2012 (Margono et al., 2014), these
733 findings support our assumptions that the observed LST increase in the Jambi province was
734 most likely caused by the observed land use changes.
735
736 To separate the effect of global warming from land-use change induced warming, we
737 considered areas with permanent and large enough forests as a reference where changes are
738 mainly because of global warming. We find that LST of forests show either no significant trends
739 (at 1:30 pm, 10:30 pm, 1:30 am) or just a clearly smaller increase of 0.03 °C per year at 10:30
740 am. The difference between the LST trend of the province and of the forest at 10:30 am was
741 0.04 °C per year, resulting in a ΔLST of 0.6 °C between the province and forest in the period
742 2000 and 2015. We point out that our MODIS analysis has a larger proportion of data from the
743 dry season compared from the wet season, as there were more cloud free conditions during the
744 dry season. Thus, our reported warming effect reflects cloud free conditions. During cloudy
745 conditions, particularly in the wet season, the warming effect is expected to be lower. A
746 seasonality analysis showed that the relationships in the dry season are stronger than for the wet
747 season (see Supporting information S10, fig. S10.1) which suggests that the warming is more
748 pronounced during the dry season compared to the wet season, which is reasonable as we have
749 more incoming radiation during the dry season.
750
751 With the warming effects we found between forest and other land cover types (ΔLST, Fig. 4a)
752 and the observed land cover changes by Clough et al. (2016), Drescher et al. (2016) (Supporting
753 Information S9, table S9.1 and S9.2) we estimated the contribution of all land cover types
754 (except forest) to the ΔLST of the province between 2000 and 2015 to be 0.51°C out of the

observed 0.6°C, which also supports our assumption that the LST increase in Jambi was for 85% driven by land cover changes (see Supporting Information 9, Table S9.1 & S9.2: Land use change analysis), with clear cut areas having a large contribution as they have the largest warming effect.

The observed small, but significant increase in LST of forests of 0.03 °C per year at 10:30 am reflects a LST change independent of land cover changes, as the forest remained unchanged over that time period. A potential driver of that LST increase is the general global air temperature trend because of changes in radiative forcing or border effects (advection from warmer land uses), which is similar to the 1994 - 2014 time series analysis of Kayet et al. (2016), who showed a LST increase for all land cover types ranging from wasted land, agriculture land, open forest, dense forest, water bodies and built up areas.

The observed trends of the provincial air temperature (Fig. 5f) were significant, suggesting that a general warming due to global and regional effects contributes to the observed warming at the provincial level during day and night time, but that it is smaller than the land cover change induced effects (Supporting Information S9, Table S9.1 & S9.2) at the provincial level (Fig. 5a and 5b).

In our long-term analysis on the regional effects of land use change we observed an increase in the mean LST and mean air temperature in the 2000 - 2015 period, concurrent with a decrease of the NDVI. The warming observed from MODIS LST data and from the air temperature obtained from the independent ERA Interim Reanalysis in the Jambi province are most likely caused by the observed decrease of the forest area and an increase of oil palm, rubber and other cash crop areas in the same period, with other effects such as radiative forcing changes and additional natural effects playing a smaller role. Given the plan of the Indonesian government

781 to substantially expand oil palm production with a projected additional demand of 1 to 28 Mha
782 in 2020 (Wicke et al., 2011), the strong warming effect we show for Jambi may serve as an
783 indication of future LST changes for other regions of Indonesia that will undergo land
784 transformations towards oil palm plantations.
785 A recent study by Tölle et al. (2017) showed that for Southeast Asia, land use change at large
786 scale may increase not only surface temperature but may impact other aspects of local and
787 regional weather and climate occurring also in regions remote from the original landscape
788 disturbance. Their results also indicate that land clearings can amplify the response to climatic
789 extreme events such as El Niño Southern Oscillation (ENSO). The observed effects of land use
790 change on the biophysical variables may have implications for ecosystem services in the Jambi
791 province beyond a pure warming effect. The high precipitation in this region in combination
792 with the reduced vegetation cover of bare land and young oil palm plantations impose risks of
793 soil erosion caused by surface run off. Less water infiltration into the soil, thereby decreasing
794 the soil water storage may lead to low water availability in the dry season (Dislich et al., 2016;
795 Merten et al., 2016). High surface temperatures in combination with low water availability may
796 make the vegetation and the surroundings more vulnerable to fires.
797
798 **5 Conclusion**
799
800 In summary, we studied the effects of land use and land cover changes on the surface
801 biophysical variables in Jambi and explained the underlying mechanisms of the surface
802 temperature regulation. We derived biophysical variables from satellite data, analyzed the
803 biophysical impacts of deforestation and on a local scale we found a general warming effect
804 after forests are transformed to cash or tree croplands (oil palm, rubber, acacia) in the Jambi
805 province of Sumatra. The warming effect after forest conversion results from the reduced
806 evaporative cooling, which was identified as the main determinant of regulating the surface

807 temperature. On a regional scale, we saw that the effects of land cover changes are reflected
808 back in changes of the LST, NDVI and air temperature in Jambi. The warming effect induced
809 by land cover change clearly exceeded the global warming effect. Understanding the effects of
810 land cover change on the biophysical variables may support policies regarding conservation of
811 the existing forests, planning and expansion of the oil palm plantations and possible
812 afforestation measures.

Supporting Information

Supporting information to this article is arranged as follows:

Author contributions. Clifton R. Sabajo conducted the research, fieldwork an analysis and prepared the manuscript, which was reviewed by Guerric le Maire, Tania June, Ana Meijide, Olivier Roupsard and Alexander Knohl. Ana Meijide and Alexander Knohl provided the meteorological data.

Competing interests. The authors declare to have no conflict of interest.

Acknowledgements. This research was funded by the Erasmus Mundus Joint Doctorate Programme Forest and Nature for Society (EMJD FONASO) and the German Research Foundation (DFG) through the CRC 990 "EFForTS, Ecological and Socioeconomic Functions of Tropical Lowland Rainforest Transformation Systems (Sumatra, Indonesia)" (subproject A03). A special thanks to Huta Julu Bagus Putra, a.k.a. Monang, for his assistance and translation during the field work in Indonesia.

References

Alkama, R. and Cescatti, A.: Biophysical climate impacts of recent changes in global forest cover, Science, 351(6273), 600–604, doi:10.1126/science.aac8083, 2016.

Ban-Weiss, G. A., Bala, G., Cao, L., Pongratz, J. and Caldeira, K.: Climate forcing and response to idealized changes in surface latent and sensible heat, Environ. Res. Lett., 6(3), 34032, 2011.

Barsi, J. A., Barker, J. L. and Schott, J. R.: An Atmospheric Correction Parameter Calculator for a Single Thermal Band Earth-Sensing Instrument, Geosci. Remote Sens. Symp. 2003 IGARSS 03 Proc. 2003 IEEE Int., 5, 3014–3016 vol.5, doi:10.1109/IGARSS.2003.1294665, 2003.

Barsi, J. A., Schott, J. R., Palluconi, F. D. and Hook, S. J.: Validation of a web-based atmospheric correction tool for single thermal band instruments, in Proc. SPIE, Earth Observing Systems X, vol. 5882, San Diego, California, USA., 2005.

Bastiaanssen, W. G. .: SEBAL-based sensible and latent heat fluxes in the irrigated Gediz Basin, Turkey, J. Hydrol., 229(1–2), 87–100, doi:10.1016/S0022-1694(99)00202-4, 2000.

Bastiaanssen, W. G. M., Menenti, M., Feddes, R. A. and Holtslag, A. A. M.: A remote sensing surface energy balance algorithm for land (SEBAL) - 1. Formulation, J. Hydrol., 212(1–4), 198–212, doi:10.1016/s0022-1694(98)00253-4, 1998a.

Bastiaanssen, W. G. M., Pelgrum, H., Wang, J., Ma, Y., Moreno, J. F., Roerink, G. J. and van der Wal, T.: A remote sensing surface energy balance algorithm for land (SEBAL).: Part 2: Validation, J. Hydrol., 212–213, 213–229, doi:10.1016/S0022-1694(98)00254-6, 1998b.

Bathiany, S., Claussen, M., Brovkin, V., Raddatz, T. and Gayler, V.: Combined biogeophysical and biogeochemical effects of large-scale forest cover changes in the MPI earth system model, Biogeosciences, 7(5), 1383–1399, doi:10.5194/bg-7-1383-2010, 2010.

Beltrán-Przekurat, A., Pielke Sr, R. A., Eastman, J. L. and Coughenour, M. B.: Modelling the effects of land-use/land-cover changes on the near-surface atmosphere in southern South America, Int. J. Climatol., 32(8), 1206–1225, doi:10.1002/joc.2346, 2012.

Bindhu, V. M., Narasimhan, B. and Sudheer, K. P.: Development and verification of a non-linear disaggregation method (NL-DisTrad) to downscale MODIS land surface temperature to the spatial scale of Landsat thermal data to estimate evapotranspiration, Remote Sens. Environ., 135, 118–129, doi:10.1016/j.rse.2013.03.023, 2013.

Boisier, J. P., de Noblet-Ducoudré, N. and Ciais, P.: Historical land-use-induced evapotranspiration changes estimated from present-day observations and reconstructed land-cover maps, Hydrol. Earth Syst. Sci., 18(9), 3571–3590, doi:10.5194/hess-18-3571-2014, 2014.

Bridhikitti, A. and Overcamp, T. J.: Estimation of Southeast Asian rice paddy areas with different ecosystems from moderate-resolution satellite imagery, Agric. Ecosyst. Environ., 146(1), 113–120, doi:10.1016/j.agee.2011.10.016, 2012.

Bright, R. M., Zhao, K., Jackson, R. B. and Cherubini, F.: Quantifying surface albedo and other direct biogeophysical climate forcings of forestry activities, Glob. Change Biol., 21(9), 3246–3266, doi:10.1111/gcb.12951, 2015.

911 Clough, Y., Krishna, V. V., Corre, M. D., Darras, K., Denmead, L. H., Meijide, A., Moser, S.,
912 Musshoff, O., Steinebach, S., Veldkamp, E., Allen, K., Barnes, A. D., Breidenbach, N., Brose,
913 U., Buchori, D., Daniel, R., Finkeldey, R., Harahap, I., Hertel, D., Holtkamp, A. M., Hörandl,
914 E., Irawan, B., Jaya, I. N. S., Jochum, M., Klarner, B., Knohl, A., Kotowska, M. M.,
915 Krashevska, V., Kreft, H., Kurniawan, S., Leuschner, C., Maraun, M., Melati, D. N.,
916 Opfermann, N., Pérez-Cruzado, C., Prabowo, W. E., Rembold, K., Rizali, A., Rubiana, R.,
917 Schneider, D., Tjitrosoedirdjo, S. S., Tjoa, A., Tscharntke, T. and Scheu, S.: Land-use choices
918 follow profitability at the expense of ecological functions in Indonesian smallholder landscapes,
919 Nat. Commun., 7, 13137, 2016.

920 Coll, C., Wan, Z. and Galve, J. M.: Temperature-based and radiance-based validations of the
921 V5 MODIS land surface temperature product, J. Geophys. Res., 114(D20), 2009.

922 Coll, C., Galve, J. M., Sanchez, J. M. and Caselles, V.: Validation of Landsat-7/ETM+ Thermal-
923 Band Calibration and Atmospheric Correction With Ground-Based Measurements, Geosci.
924 Remote Sens. IEEE Trans. On, 48(1), 547–555, doi:10.1109/TGRS.2009.2024934, 2010.

925 Costa, M. H., Yanagi, S. N. M., Souza, P. J. O. P., Ribeiro, A. and Rocha, E. J. P.: Climate
926 change in Amazonia caused by soybean cropland expansion, as compared to caused by
927 pastureland expansion, Geophys. Res. Lett., 34(7), doi:10.1029/2007GL029271, 2007.

928 Davin, E. L. and de Noblet-Ducoudré, N.: Climatic Impact of Global-Scale Deforestation:
929 Radiative versus Nonradiative Processes, J. Clim., 23(1), 97–112,
930 doi:10.1175/2009JCLI3102.1, 2010.

931 Dee, D. P., Uppala, S. M., Simmons, A. J., Berrisford, P., Poli, P., Kobayashi, S., Andrae, U.,
932 Balmaseda, M. A., Balsamo, G., Bauer, P., Bechtold, P., Beljaars, A. C. M., van de Berg, L.,
933 Bidlot, J., Bormann, N., Delsol, C., Dragani, R., Fuentes, M., Geer, A. J., Haimberger, L.,
934 Healy, S. B., Hersbach, H., Hólm, E. V., Isaksen, L., Kållberg, P., Köhler, M., Matricardi, M.,
935 McNally, A. P., Monge-Sanz, B. M., Morcrette, J.-J., Park, B.-K., Peubey, C., de Rosnay, P.,
936 Tavolato, C., Thépaut, J.-N. and Vitart, F.: The ERA-Interim reanalysis: configuration and
937 performance of the data assimilation system, Q. J. R. Meteorol. Soc., 137(656), 553–597,
938 doi:10.1002/qj.828, 2011.

939 Dislich, C., Keyel, A. C., Salecker, J., Kisel, Y., Meyer, K. M., Auliya, M., Barnes, A. D.,
940 Corre, M. D., Darras, K., Faust, H., Hess, B., Klasen, S., Knohl, A., Kreft, H., Meijide, A.,
941 Nurdiansyah, F., Otten, F., Pe'er, G., Steinebach, S., Tarigan, S., Tölle, M. H., Tscharntke, T.
942 and Wiegand, K.: A review of the ecosystem functions in oil palm plantations, using forests as
943 a reference system, Biol. Rev., doi:10.1111/brv.12295, 2016.

944 Drescher, J., Rembold, K., Allen, K., Beckschäfer, P., Buchori, D., Clough, Y., Faust, H., Fauzi,
945 A. M., Gunawan, D., Hertel, D., Irawan, B., Jaya, I. N. S., Klarner, B., Kleinn, C., Knohl, A.,
946 Kotowska, M. M., Krashevska, V., Krishna, V., Leuschner, C., Lorenz, W., Meijide, A., Melati,
947 D., Nomura, M., Pérez-Cruzado, C., Qaim, M., Siregar, I. Z., Steinebach, S., Tjoa, A.,
948 Tscharntke, T., Wick, B., Wiegand, K., Kreft, H. and Scheu, S.: Ecological and socio-economic
949 functions across tropical land use systems after rainforest conversion, Philos. Trans. R. Soc.
950 Lond. B Biol. Sci., 371(1694), doi:10.1098/rstb.2015.0275, 2016.

951 Fall, S., Niyogi, D., Gluhovsky, A., Pielke, R. A., Kalnay, E. and Rochon, G.: Impacts of land
952 use land cover on temperature trends over the continental United States: assessment using the
953 North American Regional Reanalysis, Int. J. Climatol., 30(13), 1980–1993,
954 doi:10.1002/joc.1996, 2010.

955 Feddema, J. J., Oleson, K. W., Bonan, G. B., Mearns, L. O., Buja, L. E., Meehl, G. A. and
956 Washington, W. M.: The Importance of Land-Cover Change in Simulating Future Climates,
957 Science, 310(5754), 1674, doi:10.1126/science.1118160, 2005.

958 Hoffmann, W. A. and Jackson, R. B.: Vegetation–Climate Feedbacks in the Conversion of
959 Tropical Savanna to Grassland, J. Clim., 13(9), 1593–1602, doi:10.1175/1520-
960 0442(2000)013<1593:VCFITC>2.0.CO;2, 2000.

961 Houspanossian, J., Nosetto, M. and Jobbágy, E. G.: Radiation budget changes with dry forest
962 clearing in temperate Argentina, Glob. Change Biol., 19(4), 1211–1222,
963 doi:10.1111/gcb.12121, 2013.

964 Idso, S. B. and Jackson, R. D.: Thermal radiation from the atmosphere, J. Geophys. Res.,
965 74(23), 5397–5403, doi:10.1029/JC074i023p05397, 1969.

966 Jiang, Y., Fu, P. and Weng, Q.: Assessing the Impacts of Urbanization-Associated Land
967 Use/Cover Change on Land Surface Temperature and Surface Moisture: A Case Study in the
968 Midwestern United States, Remote Sens., 7(4), doi:10.3390/rs70404880, 2015.

969 Kayet, N., Pathak, K., Chakrabarty, A. and Sahoo, S.: Spatial impact of land use/land cover
970 change on surface temperature distribution in Saranda Forest, Jharkhand, Model. Earth Syst.
971 Environ., 2(3), 1–10, doi:10.1007/s40808-016-0159-x, 2016.

972 Lawrence, D. and Vandecar, K.: Effects of tropical deforestation on climate and agriculture,
973 Nat. Clim. Change, 5(1), 27–36, 2015.

974 Lee, X., Goulden, M. L., Hollinger, D. Y., Barr, A., Black, T. A., Bohrer, G., Bracho, R., Drake,
975 B., Goldstein, A., Gu, L., Katul, G., Kolb, T., Law, B. E., Margolis, H., Meyers, T., Monson,
976 R., Munger, W., Oren, R., Paw U, K. T., Richardson, A. D., Schmid, H. P., Staebler, R., Wofsy,
977 S. and Zhao, L.: Observed increase in local cooling effect of deforestation at higher latitudes,
978 Nature, 479(7373), 384–387, doi:10.1038/nature10588, 2011.

979 van Leeuwen, T. T., Frank, A. J., Jin, Y., Smyth, P., Goulden, M. L., van der Werf, G. R. and
980 Randerson, J. T.: Optimal use of land surface temperature data to detect changes in tropical
981 forest cover, J. Geophys. Res. Biogeosciences, 116(G2), doi:10.1029/2010JG001488, 2011.

982 Li, F., Jackson, T. J., Kustas, W. P., Schmugge, T. J., French, A. N., Cosh, M. H. and Bindlish,
983 R.: Deriving land surface temperature from Landsat 5 and 7 during SMEX02/SMACEX, 2002
984 Soil Moisture Exp. SMEX02, 92(4), 521–534, doi:10.1016/j.rse.2004.02.018, 2004.

985 Li, Y., Zhao, M., Motesharrei, S., Mu, Q., Kalnay, E. and Li, S.: Local cooling and warming
986 effects of forests based on satellite observations, Nat. Commun., 6 [online] Available from:
987 http://dx.doi.org/10.1038/ncomms7603, 2015.

988 Liang, S.: Narrowband to broadband conversions of land surface albedo I: Algorithms, Remote
989 Sens. Environ., 76(2), 213–238, doi:10.1016/S0034-4257(00)00205-4, 2000.

990 Lim, Y.-K., Cai, M., Kalnay, E. and Zhou, L.: Observational evidence of sensitivity of surface
991 climate changes to land types and urbanization, Geophys. Res. Lett., 32(22),
992 doi:10.1029/2005GL024267, 2005.

993 Lim, Y.-K., Cai, M., Kalnay, E. and Zhou, L.: Impact of Vegetation Types on Surface
994 Temperature Change, J. Appl. Meteorol. Climatol., 47(2), 411–424, 2008.

995 Loarie, S. R., Lobell, D. B., Asner, G. P., Mu, Q. and Field, C. B.: Direct impacts on local
996 climate of sugar-cane expansion in Brazil, Nat. Clim. Change, 1(2), 105–109,
997 doi:10.1038/nclimate1067, 2011a.

998 Loarie, S. R., Lobell, D. B., Asner, G. P. and Field, C. B.: Land-Cover and Surface Water
999 Change Drive Large Albedo Increases in South America, Earth Interact., 15(7), 1–16, 2011b.

1000 Longobardi, P., Montenegro, A., Beltrami, H. and Eby, M.: Deforestation Induced Climate
1001 Change: Effects of Spatial Scale, PLoS ONE, 11(4), e0153357,
1002 doi:10.1371/journal.pone.0153357, 2016.

1003 Luskin, M. S., Christina, E. D., Kelley, L. C. and Potts, M. D.: Modern Hunting Practices and
1004 Wild Meat Trade in the Oil Palm Plantation-Dominated Landscapes of Sumatra, Indonesia,
1005 Hum. Ecol., 42(1), 35–45, doi:10.1007/s10745-013-9606-8, 2014.

1006 Mahmood, R., Pielke, R. A., Hubbard, K. G., Niyogi, D., Dirmeyer, P. A., McAlpine, C.,
1007 Carleton, A. M., Hale, R., Gameda, S., Beltrán-Przekurat, A., Baker, B., McNider, R., Legates,
1008 D. R., Shepherd, M., Du, J., Blanken, P. D., Frauenfeld, O. W., Nair, U. S. and Fall, S.: Land
1009 cover changes and their biogeophysical effects on climate, Int. J. Climatol., 34(4), 929–953,
1010 doi:10.1002/joc.3736, 2014.

1011 Margono, B. A., Turubanova, S., Zhuravleva, I., Potapov, P., Tyukavina, A., Baccini, A., Goetz,
1012 S. and Hansen, M. C.: Mapping and monitoring deforestation and forest degradation in Sumatra
1013 (Indonesia) using Landsat time series data sets from 1990 to 2010, Environ. Res. Lett., 7(3),
1014 34010, doi:10.1088/1748-9326/7/3/034010, 2012.

1015 Margono, B. A., Potapov, P. V., Turubanova, S., Stolle, F. and Hansen, M. C.: Primary forest
1016 cover loss in Indonesia over 2000-2012, Nat. Clim Change, 4(8), 730–735, 2014.

1017 Marlier, M. E., DeFries, R., Pennington, D., Nelson, E., Ordway, E. M., Lewis, J., Koplitz, S.
1018 N. and Mickley, L. J.: Future fire emissions associated with projected land use change in
1019 Sumatra, Glob. Change Biol., 21(1), 345–362, doi:10.1111/gcb.12691, 2015.

1020 Meijide, A., Röll, A., Fan, Y., Herbst, M., Niu, F., Tiedemann, F., June, T., Rauf, A., Hölscher,
1021 D. and Knohl, A.: Controls of water and energy fluxes in oil palm plantations: Environmental
1022 variables and oil palm age, Agric. For. Meteorol., 239, 71–85,
1023 doi:10.1016/j.agrformet.2017.02.034, 2017.

1024 Merten, J., Röll, A., Guillaume, T., Meijide, A., Tarigan, S., Agusta, H., Dislich, C., Dittrich,
1025 C., Faust, H., Gunawan, D., Hein, J., Hendrayanto, Knohl, A., Kuzyakov, Y., Wiegand, K. and
1026 Hölscher, D.: Water scarcity and oil palm expansion: social views and environmental processes,
1027 Ecol. Soc., 21(2), doi:10.5751/ES-08214-210205, 2016.

1028 Miettinen, J., Shi, C. and Liew, S. C.: Deforestation rates in insular Southeast Asia between
1029 2000 and 2010, Glob. Change Biol., 17(7), 2261–2270, 2011.

1030 Miettinen, J., Hooijer, A., Wang, J., Shi, C. and Liew, S. C.: Peatland degradation and
1031 conversion sequences and interrelations in Sumatra, Reg. Environ. Change, 12(4), 729–737,
1032 doi:10.1007/s10113-012-0290-9, 2012.

1033 Mildrexler, D. J., Zhao, M. and Running, S. W.: A global comparison between station air
1034 temperatures and MODIS land surface temperatures reveals the cooling role of forests, J.
1035 Geophys. Res. Biogeosciences, 116(G3), doi:10.1029/2010JG001486, 2011.

1036 Nosetto, M. D., Jobbágy, E. G. and Paruelo, J. M.: Land-use change and water losses: the case
1037 of grassland afforestation across a soil textural gradient in central Argentina, Glob. Change
1038 Biol., 11(7), 1101–1117, doi:10.1111/j.1365-2486.2005.00975.x, 2005.

1039 Oliveira, L. J. C., Costa, M. H., Soares-Filho, B. S. and Coe, M. T.: Large-scale expansion of
1040 agriculture in Amazonia may be a no-win scenario, Environ. Res. Lett., 8(2), 24021, 2013.

1041 Paterson, R. R. M., Kumar, L., Taylor, S. and Lima, N.: Future climate effects on suitability for
1042 growth of oil palms in Malaysia and Indonesia, Sci. Rep., 5, 14457, 2015.

1043 Peng, S.-S., Piao, S., Zeng, Z., Ciais, P., Zhou, L., Li, L. Z. X., Myneni, R. B., Yin, Y. and
1044 Zeng, H.: Afforestation in China cools local land surface temperature, Proc. Natl. Acad. Sci.,
1045 111(8), 2915–2919, 2014.

1046 Pongratz, J., Bounoua, L., DeFries, R. S., Morton, D. C., Anderson, L. O., Mauser, W. and
1047 Klink, C. A.: The Impact of Land Cover Change on Surface Energy and Water Balance in Mato
1048 Grosso, Brazil, Earth Interact., 10(19), 1–17, 2006.

1049 Salazar, A., Baldi, G., Hirota, M., Syktus, J. and McAlpine, C.: Land use and land cover change
1050 impacts on the regional climate of non-Amazonian South America: A review, Glob. Planet.
1051 Change, 128, 103–119, doi:10.1016/j.gloplacha.2015.02.009, 2015.

1052 Salazar, A., Katzfey, J., Thatcher, M., Syktus, J., Wong, K. and McAlpine, C.: Deforestation
1053 changes land–atmosphere interactions across South American biomes, Glob. Planet. Change,
1054 139, 97–108, doi:10.1016/j.gloplacha.2016.01.004, 2016.

1055 Sheil, D., Casson, A., Meijaard, E., Van Noordwjik, M., Gaskell, J., Sunderland-Groves, J.,
1056 Wertz, K. and Kanninen, M.: The impacts and opportunities of oil palm in Southeast Asia: What
1057 do we know and what do we need to know?, Center for International Forestry Research
1058 (CIFOR), Bogor, Indonesia., 2009.

1059 Silvério, D. V., Brando, P. M., Macedo, M. N., Beck, P. S. A., Bustamante, M. and Coe, M. T.:
1060 Agricultural expansion dominates climate changes in southeastern Amazonia: the overlooked
1061 non-GHG forcing, Environ. Res. Lett., 10(10), 104015, 2015.

1062 Snyder, W. C., Wan, Z., Zhang, Y. and Feng, Y.-Z.: Classification-based emissivity for land
1063 surface temperature measurement from space, Int. J. Remote Sens., 19(14), 2753–2774,
1064 doi:10.1080/014311698214497, 1998.

1065 Sobrino, J. A., Jiménez-Muñoz, J. C. and Paolini, L.: Land surface temperature retrieval from
1066 LANDSAT TM 5, Remote Sens. Environ., 90(4), 434–440, doi:10.1016/j.rse.2004.02.003,
1067 2004.

1068 Sobrino, J. A., Jiménez-Muñoz, J. C., Zarco-Tejada, P. J., Sepulcre-Cantó, G. and de Miguel,
1069 E.: Land surface temperature derived from airborne hyperspectral scanner thermal infrared data,
1070 Remote Sens. Environ., 102(1–2), 99–115, doi:10.1016/j.rse.2006.02.001, 2006.

1071 Sobrino, J. A., Jimenez-Muoz, J. C., Soria, G., Romaguera, M., Guanter, L., Moreno, J., Plaza,
1072 A. and Martinez, P.: Land Surface Emissivity Retrieval From Different VNIR and TIR Sensors,

1073 Geosci. Remote Sens. IEEE Trans. On, 46(2), 316–327, doi:10.1109/TGRS.2007.904834,
1074 2008.

1075 Spracklen, D. V., Arnold, S. R. and Taylor, C. M.: Observations of increased tropical rainfall
1076 preceded by air passage over forests, Nature, 489(7415), 282–285, doi:10.1038/nature11390,
1077 2012.

1078 Tölle, M. H., Engler, S. and Panitz, H.-J.: Impact of Abrupt Land Cover Changes by Tropical
1079 Deforestation on Southeast Asian Climate and Agriculture, J. Clim., 30(7), 2587–2600,
1080 doi:10.1175/JCLI-D-16-0131.1, 2017.

1081 Verstraeten, W. W., Veroustraete, F. and Feyen, J.: Estimating evapotranspiration of European
1082 forests from NOAA-imagery at satellite overpass time: Towards an operational processing
1083 chain for integrated optical and thermal sensor data products, Remote Sens. Environ., 96(2),
1084 256–276, doi:10.1016/j.rse.2005.03.004, 2005.

1085 Vlassova, L., Perez-Cabello, F., Nieto, H., Martín, P., Riaño, D. and de la Riva, J.: Assessment
1086 of Methods for Land Surface Temperature Retrieval from Landsat-5 TM Images Applicable to
1087 Multiscale Tree-Grass Ecosystem Modeling, Remote Sens., 6(5), doi:10.3390/rs6054345,
1088 2014.

1089 Voogt, J. A. and Oke, T. R.: Effects of urban surface geometry on remotely-sensed surface
1090 temperature, Int. J. Remote Sens., 19(5), 895–920, doi:10.1080/014311698215784, 1998.

1091 Wan, Z., Zhang, Y., Zhang, Q. and Li, Z.-L.: Quality assessment and validation of the MODIS
1092 global land surface temperature, Int. J. Remote Sens., 25(1), 261–274,
1093 doi:10.1080/0143116031000116417, 2004.

1094 Wang, J., Pan, F., Soininen, J., Heino, J. and Shen, J.: Nutrient enrichment modifies
1095 temperature-biodiversity relationships in large-scale field experiments, Nat. Commun., 7,
1096 13960, doi:10.1038/ncomms13960, 2016.

1097 Weng, Q.: Thermal infrared remote sensing for urban climate and environmental studies:
1098 Methods, applications, and trends, ISPRS J. Photogramm. Remote Sens., 64(4), 335–344,
1099 doi:10.1016/j.isprsjprs.2009.03.007, 2009.

1100 Weng, Q., Lu, D. and Schubring, J.: Estimation of land surface temperature–vegetation
1101 abundance relationship for urban heat island studies, Remote Sens. Environ., 89(4), 467–483,
1102 doi:10.1016/j.rse.2003.11.005, 2004.

1103 Wicke, B., Sikkema, R., Dornburg, V. and Faaij, A.: Exploring land use changes and the role
1104 of palm oil production in Indonesia and Malaysia, Land Use Policy, 28(1), 193–206, 2011.

1105 Wukelic, G. E., Gibbons, D. E., Martucci, L. M. and Foote, H. P.: Radiometric calibration of
1106 Landsat Thematic Mapper thermal band, Remote Sens. Environ., 28(0), 339–347,
1107 doi:10.1016/0034-4257(89)90125-9, 1989.

1108 Yue, W., Xu, J., Tan, W. and Xu, L.: The relationship between land surface temperature and
1109 NDVI with remote sensing: application to Shanghai Landsat 7 ETM+ data, Int. J. Remote Sens.,
1110 28(15), 3205–3226, doi:10.1080/01431160500306906, 2007.

1111 Zhang, Z. and He, G.: Generation of Landsat surface temperature product for China, 2000–
1112 2010, Int. J. Remote Sens., 34(20), 7369–7375, doi:10.1080/01431161.2013.820368, 2013.

1113 Zhou, X. and Wang, Y.-C.: Dynamics of Land Surface Temperature in Response to Land-
1114 Use/Cover Change, Geogr. Res., 49(1), 23–36, doi:10.1111/j.1745-5871.2010.00686.x, 2011.

1115